Probing the limits of quantum mechanics using a cold mechanical force sensor

Plugge, J.

Chapter 5

Experimental Results Towards Detecting a Single Electron using Magnetic Resonance Force Microscopy

The ability to couple a macroscopic resonator to a *single* electron opens the possibility to test the limit on superpositions, if any. However, as the magnetic field of the magnet at the tip of the force sensor is macroscopic, it interacts with a lot of spins. At the same time, all these spins will affect the resonator. In order to test this influence and to try to determine the amount of spins, we use our force sensor as a magnetic force microscope. By recording the cantilever resonance frequency and Q-factor, we obtain information about the spins in the sample. This type of measurement has already been done before in our group [54, 55] on a diamond that was specified to have less than 1 ppm of nitrogen impurities. However, even if the experiments conclude the bulk spin density was 0.4 ppm and the surface spin density was found to be 0.06 spins/nm^2, it was still too high for the quantum experiments we aim to conduct. For this reason we test a thin diamond sample, that we put on top of the detection chip, and is advertised to have on the order of 5 ppb nitrogen impurities. We conclude that the surface spin density is 0.02 spins/nm^2, two times lower than our lowest surface spin density so far, and that the bulk spin density is 54 ppb, ten times lower than than the bulk spin density found on a previous diamond sample. We find that the T_1 time of the surface spin density is similar to previously found values of 0.5 ms. This has detrimental effect on the cantilever dissipation. To improve this, we discuss the addition of an external magnetic field and the influence it has on the spins and cantilever characteristics.

5.1 Introduction

The detection of a single spin using Magnetic Resonance Force Microscopy is not new, as it has already been done before by Rugar *et al.* [6] in 2004. Their setup differs from our intended experiment in a seemingly trivial way, their results were obtained at 1.6 K while we aim to conduct the experiment at around 1 mK, in order to allow for future quantum experiments. This, however, requires some changes to the setup. To reduce the heat dissipated in the experiment, the cantilever motion cannot be detected using a laser interferometer anymore and the microwave coil has to dissipate less heat while sending the GHz B_1-pulses needed to excite the electron spin.

As explained in section 2.2.2, the laser interferometer in the setup of Rugar *et al.* is replaced by a detection circuit connecting to a SQUID. Considering the mentioned subpar coupling between the pick-up loop and the SQUID, the cantilever needs to be close to the pick-up loop to have sufficient sensitivity to observe the thermal motion of the cantilever. Additionally, we need to avoid the interaction between the cantilever magnet and the superconducting strip lines on top of the detection chip. The optimal position to conduct the experiment is thus defined by a position far enough from the pick-up loop and RF line to avoid unintended behavior due to the Meissner effect, but close enough to be able to detect cantilever motion and to obtain sufficient B_1-field. Furthermore, that position needs to be close to a single spin inside the sample. Finally, we need to have a sufficiently low amount of surface spins on the surface of the sample.

This chapter will elaborate further on the setup of the nv mrfm and the sample placed into it. The density of surface spins on top of the sample will be determined and compared to the values of diamond samples our group has previously investigated. We end by discussing the effect of an external magnetic field.

5.2 Methodology

The nv mrfm (figure 5.1) is designed around the detection chip which is placed on top of a Niobium flux-concentrator electromagnet. For a more elaborate description of the detection circuit, we refer to section 2.2.2. In the zoomed in picture of the sample in figure 5.1, the RF line is shown. The RF line ends in wirebond pads from where four wirebonds on both sides connect the chip to superconducting semi-rigids. In addition to the flux change picked up by the pick-up loop due to the cantilever motion, the

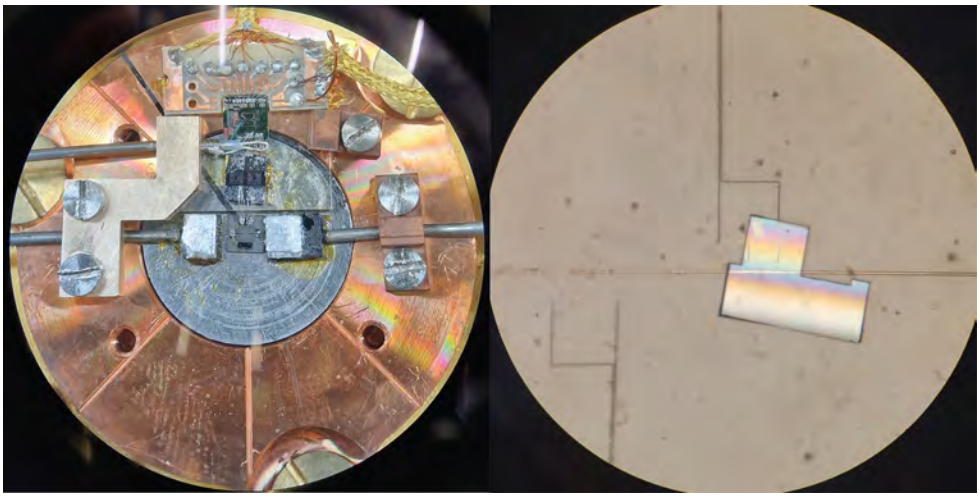

Figure 5.1: Pictures of the nv mrfm sample holder. On the *left* picture the full sample holder is shown, with the detection chip in the middle on top of the external field magnet. The RF wires come from the east and west towards the detection chip. Towards the north of the detection chip we have the transformer chip, a RF compensation loop and the SQUID chip respectively. On the *right* picture a zoom-in of the detection chip is shown with the diamond sample on top of the pick-up loop.

RF-pulses will also be picked up by the pick-up loop and will thus be detected by the SQUID. To reduce the unwanted effects due to the RF current induced flux, a compensation loop is added in between the SQUID chip and the transformer chip. The idea is to reduce the SQUID response to the RF-pulses sent through the RF line, by sending the same RF frequency with optimized amplitude and phase through this compensation loop to null out the response. A similar setup for flux compensation has already been tested by Martin de Wit *et al.* [65] in 2019 for MHz frequencies, rather than for GHz frequencies. In the MHz approach a compensation signal could be sent to a line on the SQUID chip. Because of on-chip filters this is not possible for GHz signals. Hence the use of a GHz loop close to the chips.

5.2.1 Diamond Sample

The sample placed on top of the diamond detection chip is obtained from the Hanson group in Delft. It is thinned by etching, and fabricated from a starting material specified to have fewer nitrogen impurities than 5 ppb [66]. The sample should have a low density of spins, as ideally, the coupled electron spin should not have any interaction with neighboring electron spins.

When the cantilever is brought closer to the sample, the magnet at the tip of the cantilever will exert a force on the spins that depends on the gradient of the magnet. In the same way, the spins will exert a force on the cantilever causing it to change its resonance frequency f_0 estimated to be

$$\Delta f = \frac{1}{2}\frac{f_0}{k_0}\vec{\mu}\cdot\frac{\partial^2\vec{B}(\vec{r})}{\partial x^2}, \tag{5.1}$$

with k_0 the spring constant of the isolated cantilever, $\vec{B}(\vec{r})$ the magnetic field of the magnet at position $\vec{r}$ and x the direction of cantilever motion. This equation assumes that $\vec{\mu}$ does not depend on the cantilever motion, but as shown by de Voogd *et al.* [8] the spin gets influenced by the motion of the cantilever which induces a subtle frequency shift and opens a dissipation channel affecting the Q-factor, especially when the T_1 time of the spins gets more comparable to $(2\pi f_0)^{-1}$. We differentiate between two types of spins that couple to the cantilever, bulk spins and surface spins. The main contribution of bulk spins consist of defects in the diamond that that are called the P1 and P2 defects. Both of these defects exist due to nitrogen impurities and are spin $\frac{1}{2}$ systems. Since dilute bulk electron spins have T_1-times that have been measured to be in the order of seconds [67] at low temperatures $< 50\,\mathrm{K}$, we do not expect them to affect the Q-factor. Using the results obtained from the full calculations done by de Voogd *et al.* [8], we obtain for the surface spins

$$\begin{aligned}\Delta f_{\mathrm{surface}} &= \frac{f_0}{2k_0}\frac{\sigma\mu_e^2}{k_BT}C_{\mathrm{surface}}\frac{(2\pi f_0T_1)^2}{1+(2\pi f_0T_1)^2}\\ \Delta\frac{1}{Q}_{\mathrm{surface}} &= \frac{1}{k_0}\frac{\sigma\mu_e^2}{k_BT}C_{\mathrm{surface}}\frac{2\pi f_0T_1}{1+(2\pi f_0T_1)^2},\end{aligned} \tag{5.2}$$

with σ the surface spin density, μ_e the electron magnetic moment, k_B the Boltzmann constant and T the temperature. The contribution from the surface spins C_{surface} is obtained from a surface integral

$$C_{\mathrm{surface}} = \iint_S d^2r\frac{|\frac{d}{dx}\vec{B}_{||\vec{B}_0}|^2}{\cosh^2(\frac{\mu_eB_0}{k_BT})}, \tag{5.3}$$

where $\frac{d}{dx}\vec{B}_{||\vec{B}_0}$ denotes the full derivative of the magnetic field vector to x parallel to the magnetic field vector $\vec{B}_0$ and B_0 the absolute value of the magnetic field at every position. The contribution of bulk spins is given by

$$\begin{aligned}\Delta f_{\mathrm{bulk}} &= \frac{f_0}{2k_0}\frac{\rho\mu_e^2}{k_BT}C_{\mathrm{bulk}}\\ \Delta\frac{1}{Q}_{\mathrm{bulk}} &= 0,\end{aligned} \tag{5.4}$$

with ρ the bulk spin density and

$$C_{\text{bulk}} = \iiint_V d^3r \frac{|\frac{d}{dx}\vec{B}_{||\vec{B}_0}|^2}{\cosh^2(\frac{\mu_e B_0}{k_B T})}. \tag{5.5}$$

In order to obtain the values for the surface spin density σ, the bulk spin density ρ and the T_1 time of the surface spins we fit the functions

$$\begin{aligned} f &= f_0 + \Delta f_{\text{surface}} + \Delta f_{\text{bulk}} \\ Q &= \left(\frac{1}{Q}_0 + \Delta \frac{1}{Q}_{\text{surface}}\right)^{-1} \end{aligned} \tag{5.6}$$

to a dataset of cantilever resonance frequency and Q-factor as a function of distance to the sample and temperature.

5.2.2 Data collection

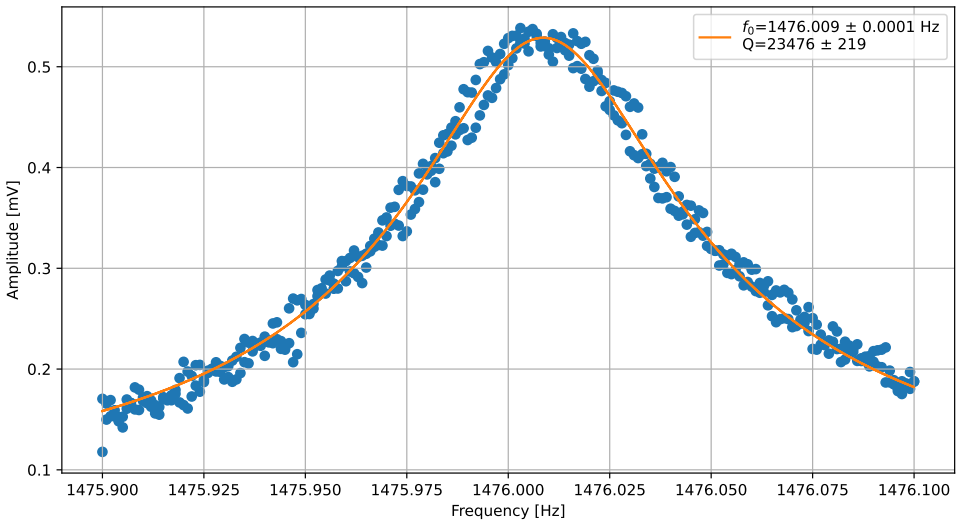

Figure 5.2: Example of a cantilever sweep done at a height of $z \approx 6\,\mu$m and a temperature of $T = 60\,$mK. The data is fit to a Lorentzian in Python using the curve_fit function from the scipy library. The value and error are obtained from the mean and standard deviation respectively by bootstrapping and then fitting the data set a thousand times.

The values for resonance frequency and Q-factor are obtained from cantilever sweeps using a dither piezo glued on the cantilever mount close to the cantilever. By exciting this piezo at the resonance frequency of the cantilever, the cantilever

motion gets amplified. Conducting a frequency sweep around the expected cantilever frequency and fitting the result to a Lorentzian provides a method to determine the resonance frequency and Q-factor of which the reliability depends on the carefulness of the user. The frequency sweeps are conducted in both directions and care is taken to prevent for non-linear effects. Because of the lock-in time constant and the high cantilever Q, the fit of the resonance frequency depends on the sweep direction. Therefore, a Lorentzian fit is done to both frequency directions separately; the Q-factor and resonance frequency are then obtained from the mean of both fits. An example of a frequency sweep including the fit is shown in figure 5.2.

The error in the fit values was obtained from a bootstrapping procedure. We randomly pick data (same amount as the dataset, with replacement) from the dataset and use this random dataset to fit a Lorentzian to. This procedure is then repeated a thousand times, every time picking random data again and fitting a Lorentzian yielding us a list of fit values. From the mean and standard deviation we obtain the 'real' fit value and error respectively.

5.3 Results and discussion

The frequency sweeps are conducted at eleven different temperatures, ranging between 60 mK and 800 mK at seven different heights. For every temperature and almost every height, we also conducted a sweep at three different drive amplitudes which are 2, 5 and 10 mV. The exact positions and available data for every drive amplitude is presented in figure 5.3. The full dataset that consists of the resonance frequency and Q-factor versus height and temperature is then fitted to equation 5.6. However, as the same frequency shift can be obtained from a large contribution of bulk spins and lower contribution of surface spins as for a large contribution of surface spins and low contribution of bulk spins, we have to be careful in fitting the data. Furthermore, as the term $(2\pi f_0 T_1)^2/[1+(2\pi f_0 T_1)^2] \approx 1$ for $(2\pi f_0 T_1) \gg 1$, the T_1 time does not have a big influence on the frequency shift. In order to decrease the amount of dependent variables, we thus keep the T_1 time constant for the frequency shift optimization. The T_1 value that should be used for the fits can be obtained from the dataset, as from equation 5.2 we find, for the case that frequency shift from surface spins is much larger than the frequency shift of the bulk spins, that

$$\frac{\Delta f_{\text{surface}}/f_0}{\Delta \frac{1}{Q}_{\text{surface}}} = \pi f_0 T_1. \tag{5.7}$$

Thus, by dividing the frequency shift data by the Q-factor data and taking the mean, we obtain a value for T_1 which was found to be 0.5 ms. Using this value for T_1, we

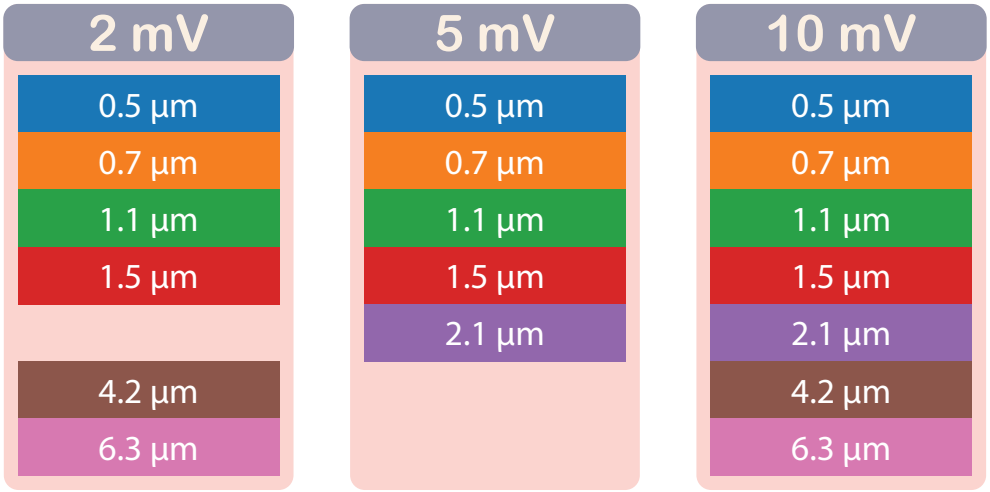

Figure 5.3: The measured data for every drive amplitude. We only have a full dataset for a drive amplitude of 10 mV.

obtain $(2\pi f_0 T_1)^2/[1+(2\pi f_0 T_1)^2] \approx 0.96$. We thus accept a 5 % error on the values obtained from the optimization algorithm.

5.3.1 Fit results

We first fit the different heights separately in order to obtain f_0 for every height. We assume f_0 is different for different heights because the lateral position of the cantilever does vary by $\pm 1.5\,\mu$m as the height varies. The highest contribution for frequency shift is expected from spins closest to the cantilever, thus similarly the largest spin contribution is expected for the temperature sweep with the cantilever closest to the sample. For this reason, we take the value found for the bulk spin density (ρ) from the dataset closest to the sample ($0.5\,\mu$m) and use this ρ to optimize for the surface spin density (σ) on multiple heights at the same time. Afterwards, we use the obtained value for σ and use this to optimize ρ on multiple heights at the same time.

By using this procedure, we observed a overestimation of ρ (64 ppb) when fitting on the whole dataset. Thus, we started to investigate the influence of every height dataset on the obtained values for σ and ρ. Above sequence was repeated for different amounts of included data in the fits, resulting in different values for ρ which are then plotted in figure 5.4. From this, we find that the overestimation mainly results from including $4.2\,\mu$m and $6.3\,\mu$m in the fitting procedure. As we aim to include as much data as possible in the fitting procedure, but at the same time try to obtain

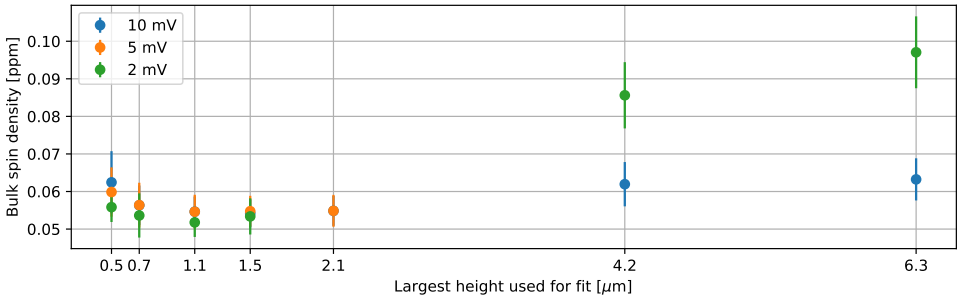

Figure 5.4: The obtained value of the bulk spin density (ρ) for different amounts of included datasets for height and drive amplitude.

reproducible results, we will include the first four heights in our fitting procedure. This choice is based on it being the highest amount of included data for which the different drive amplitudes agree within their error on the optimized value for ρ.

Next, we use the obtained σ to optimize T_1 on the Q-factor data. Like before, we first fit for every height separately to obtain the different values of Q_0 for every height. These are then used to optimize T_1 on the full dataset. The values for the

	first guess	value	error	unit
σ	0.06	0.020	0.0003	spins/nm^2
ρ	5	54	2.6	ppb
T_1	0.5	0.44	0.005	ms

Table 5.1: The optimized parameters obtained from the fits.

surface spin density, bulk spin density and T_1 are presented in table 5.1, the data and fits are presented in figure 5.5.

5.3.2 Discussion

The presented data does not include one temperature sweep we conducted at a height of 1.1 μm, as in this dataset the frequency shift was in the other direction. In order to investigate this and to check the reproducibility, we conducted an extra measurement at 1.1 μm which is the one presented in figure 5.5. Since formulas 5.2 and 5.4 can only account for positive frequency shift, the presented model is not able to explain the measured data. Because the second time we measured at a height of 1.1 μm we did

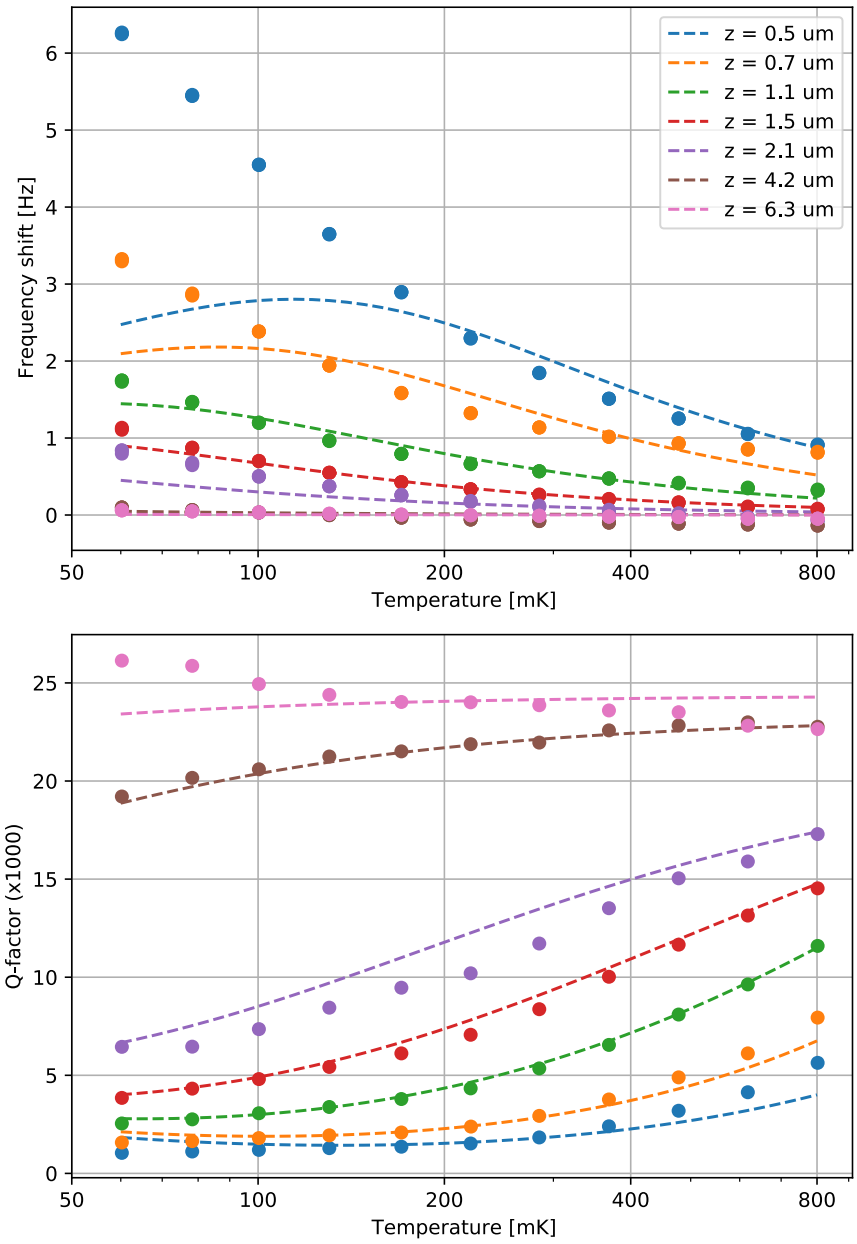

Figure 5.5: The data and fits for the frequency shift and Q-factor as a function of temperature for different heights. The measured resonance frequencies were in the 1475 to 1482 Hz range.

not see the ununderstood sign, this temperature sweep is not included in the analysis described in subsection 5.3.1. In case one ever experiences the same phenomenon or is interested in further investigation, the data is presented in figure 5.6.

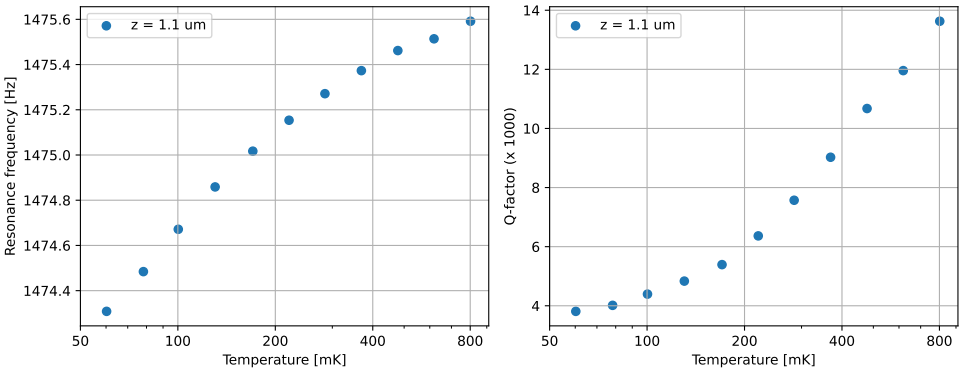

Figure 5.6: Frequency shift and Q-factor as a function of temperature, this is the only temperature sweep where we observed a negative frequency shift when lowering the temperature.

Figures 5.5 and 5.6 also show there are effects other than the presented model that can influence the Q-factor and (mainly) the resonance frequency. This model does, for example, not include electrostatic effects or noise sources arising from cables or other experiments inside the cryostat. Also, the model assumes an infinitely large surface, while the crystal under investigation has finite size. These could have affected all measurements and may also explains why we cannot fit the data perfectly. It seems the cantilever felt an additional restoring force (or absence of a negative restoring force) on top of the spin contribution causing its resonance frequency to rise further and for lower temperatures than the model predicts. Furthermore, the restoring force seems to also be temperature dependent, suggesting it can not only be explained by electrostatic forces.

As multiple combinations of values for the bulk spin density and surface spin density will be able to fit the data, the choice for the first guesses have some influence on the end result. As for the bulk spin density, the first guess is taken to be the upper bound of the value advertised by the manufacturer. For the surface spin density, we did not have a value that had been tested before on our sample. That is the reason we resorted to using the value measured by De Wit *et al.* [55], as this was also tested on diamond. As an extra check, we also run the optimization with a first guess based on the value obtained by De Voogd in his dissertation [18] ($0.072\,\mathrm{spins/nm^2}$) which yielded the same values for both spin densities within their error.

The height above the sample also introduces some uncertainty. As described, we use a capacitive reading in order to determine the position of the cantilever magnet. Despite our efforts in lowering the noise on the measurement of the capacitance, we have not been able to lower the noise enough to know the position with a higher certainty than shown in the figures (order 100 nm). The height of the sample surface was determined by lowering the position of the magnet until the resonance of the cantilever was not visible anymore. Combined, we thus have an uncertainty on every position together with a global uncertainty arising from the the sample height determination.

Additionally, there is also uncertainty on the lateral positions, as is shown in figure 5.7. From this figure (in combination with figure 5.8) we see that the two

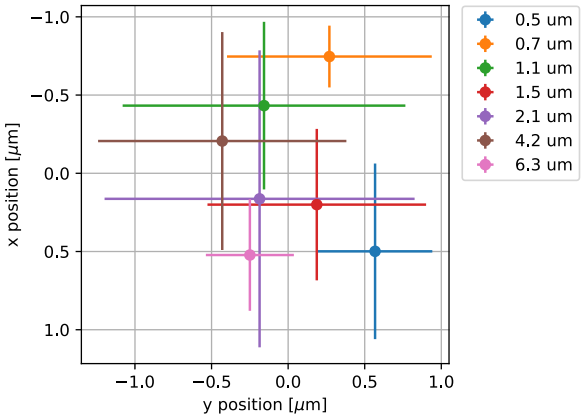

Figure 5.7: The lateral positions for every height measurement. In order to be consistent with the orientation of other figures in this chapter, the x and y-axes are rotated by 90 degrees. The origin here is taken as the mean value of the lateral positions. In this coordinate system, the closest pick-up loop line runs along $y = -10.7\,\mu$m, so still more than $9\,\mu$m away from the closest measurement. Even though the measurements are at the largest possible separation $2\,\mu$m apart, all still fall within the (to scale) sketched magnet in figure 5.8.

measurements closest to the sample (blue and orange) are both closer to the edge of the sample. As the edge of the sample can have an additional amount of dangling bonds that can influence the cantilever characteristics, it may be part of the reason that the frequency shift of both measurements is higher than the model presented predicts. However, it cannot be the full explanation, as the frequency shift at these heights seems to get larger as the temperature goes down. In order to verify this, the measurements should be repeated at lower temperatures to study if the frequency shift gets smaller again for lower temperatures, as the model predicts.

Furthermore, equations 5.6 assume a surface that extends infinitely in the lateral directions together with a bulk sample below it that has infinite thickness. For the experiments on spin density of a sample done before in our group [54, 55] these assumptions were valid, since the chip they determined the spin density of was on the order of $100 - 1000$ magnet diameters in size. But, as shown in figure 5.1, our sample is on the widest and tallest parts only on the order of 15 and 10 diameters in size, respectively. To make matters worse, we cannot just choose to conduct our measurement in the middle of this sample as we require sufficient coupling to the pick-up loop. For this reason, the described measurement was conducted close to the corner of the sample as this place was on the sweet spot considering coupling, Meissner effects resulting from the superconducting pick-up loop lines and the edge of the sample. Figure 5.8 shows a sketch of the conducted experiment.

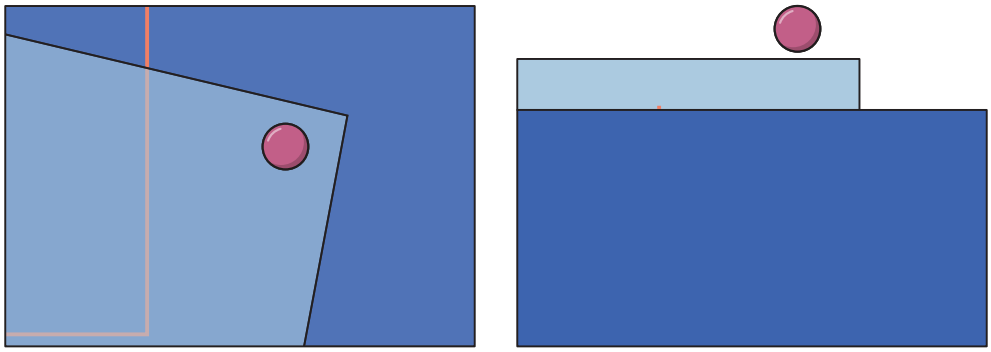

Figure 5.8: A to scale sketch of the experiment conducted in this chapter, from a top view (*left*) and from the front (*right*). The magnet at the tip of the cantilever (pink) is one diameter away from the edge of the diamond sample (light blue) which lies on top of the detection chip (dark blue) which has the pick-up loop (light orange) on it.

The described caveats should impose some caution in taking the optimized values as facts. For future experiments, we are interested in a ballpark figure on the spin densities, which is the reason why we accept these uncertainties. Regarding the obtained values, the diamond sample used in the experiment was advertised to have impurities lower than 5 ppb. Our value for $\rho = 54 \pm 3$ ppb seems to disagree with this value. As an additional analysis, we can take into account that the diamond sample is only about $4\,\mu$m thick, with a diamond detection chip underneath. In order to calculate the contribution of the detection chip, we approximate the bulk spin density of the detection chip by the value found on a similar chip tested by de Wit *et al.* [55], which was 0.4 ppm. By setting the bulk spin density to 0.4 ppm for the spin contribution from the detection chip, we find a lowered bulk spin density for the diamond sample that comes out to be 52 ppb, still a factor ten higher than

the expected upper bound. Additionally, the full optimization procedure was also repeated using 5 ppb as an upper bound on the fits, this however just resulted in the fits all yielding $\rho = 5$ ppb. This means the fit to the data improved when using larger values for ρ. As for the surface spin density, the value was determined to be $\sigma = 0.020 \pm 0.0003\,\text{spins/nm}^2$, which is about a factor three lower than obtained by De Wit *et al.* [55] on a different diamond sample. We attribute the lower surface spin density partly to this being a cleaner diamond sample, as Ruf *et al.* [66] have described etching the sample in order to minimize surface contamination.

5.3.3 External magnet

The cantilever characteristics are mainly affected by spins that rotate to align with the changing magnetic field from the cantilever magnet. This energy then gets dissipated through spin-lattice relaxation, being a big cause of the drop in Q-factor. In an attempt to lower this type of energy dissipation, one could apply an external magnetic field that aligns with the cantilever magnetic moment to avoid the cantilever from deflecting by a significant amount. As the spins feel a larger static magnetic field with respect to the changing magnetic field, the energy dissipation effect will get smaller due to the spin not constantly realigning anymore. In figure 5.9 we present a simulation with different external magnetic field magnitude for a cantilever magnet at 500 nm above a diamond sample. This simulation uses the same formulas 5.3 and 5.5, but now $\frac{d}{dx}B_{||\vec{B}_0}$ includes an external field. Note that although usually a homogeneous field does not affect the derivative of the field, here it does, because the additional external field B_{ext} affects the definition of the direction B_0. The blue lines in this figure are thus the extended versions of the same colored dashed lines in figure 5.5. This shows that for a cantilever that behaves according to the presented model, an external magnetic field could greatly improve the Q-factor.

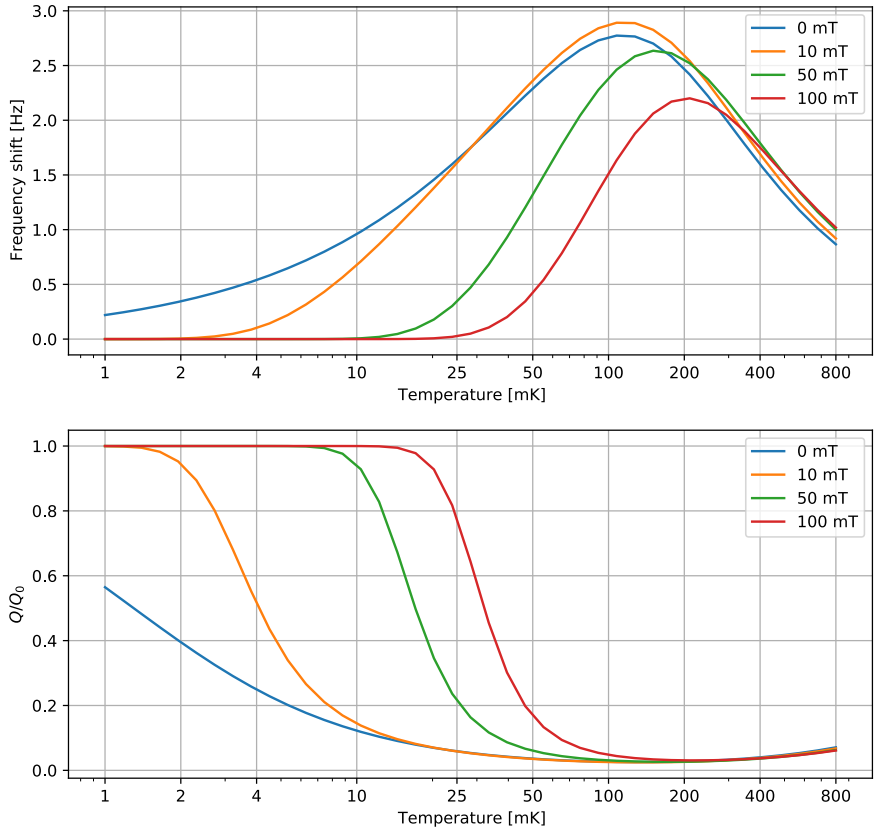

Figure 5.9: Simulation using equations 5.2 and 5.4 when a homogeneous external magnetic field is applied in the z-direction, parallel to the magnetization of the magnet. The Q-factor here is divided by the Q_0, which is defined as the Q-factor of the cantilever when it is not coupled to spins.

5.4 Conclusion and outlook

Using a mechanical force sensor, we have been able to measure the spin density of a diamond sample. As the presented experiment introduces multiple uncertainties, the presented spin densities should be interpreted as ballpark figures. The data shows that additional spins have a large effect on the cantilever. In the experiment we aim to conduct in the future, we aim to couple the force sensor to a single electron spin. Before this can be done, some changes have to made. From figure 5.5 we see that the Q-factor collapses when close to the sample and that this collapse can for a large part be explained by the presented model. The explanation for the drop in Q-factor is

spins having a T_1 time close enough to the cantilever period that energy can dissipate through these spins. In other words, they drag the cantilever by constantly realigning with its magnetic field. However, if the spins feel an additional magnetic field, larger than the magnetic field arising from the force sensor, they will align with that field instead of following the moving cantilever field. Using an external magnetic field, it should thus be possible to minimize the drop in Q-factor due to the additional spins.